Sensors and Materials, Vol. 18, No. 6 (2006) 313–327
MYU Tokyo

S & M 0652

1–10 μm PZT Films Grown by Modified Sol-Gel Method

Yi-Chu Hsu*

Department of Mechanical Engineering, Southern Taiwan University of Technology, Tainan 710, Taiwan

(Received March 20, 2006; accepted September 1, 2006)

Key words: PZT thick films, piezoelectricity MEMS, microsystems, PZT microfabrications

Lead zirconate titanate (PZT), a piezoelectric material, has a wide variety of applications in the fields of capacitors, memories, sensors and actuators owing to its excellent piezoelectric effects. There are limits to PZT films: cracking, electric leakage, small vibration displacement and sensing signals. The objective of this work is to fabricate and characterize crack-free, reliable-sensitivity, high-actuation PZT films for microsensors and microactuators. Two techniques were applied to improve conventional sol-gel processing: precursor concentration modulation and rapid thermal annealing. This research demonstrates that the former could increase both grain size and film thickness, whereas the latter could prevent film cracking. By these methods, the thickness of each coating layer is approximately 0.6 μm, and the PZT films attain a 10 μm thickness by a sixteen-coating process. The structure, surface morphology and physical properties of the PZT films were characterized by X-ray diffraction (XRD), scanning electron microscopy (SEM), atomic force microscopy (AFM), and electrical property and dynamic performance measurements. The results showed that the films were dense and crack-free, and had grain sizes between 10 and 20 μm. Also, the thicker films attained larger grain sizes. The average roughness was 2.2 nm within a surface area of 5×5 μm. At 1 kHz, the dielectric constant was approximately 160. The remnant polarization and coercive field of the PZT ferroelectric capacitors were approximately 3.63 μC/cm^2 and 64.4 kV/cm, respectively. Actuation and sensing tests were developed to measure dynamic performance. The frequencies of the first two modes in the experiments were also compared with the theoretical results obtained by considering the Euler-Bernoulli beam theory. This comparison demonstrates that the experimental results are similar to the theoretical data with an error of 5.19% at the first resonance.

1. Introduction

Piezoelectric materials are very popular owing to their many desirable properties. First, they can transform electrical signals into mechanical deformation (i.e., they can serve as an

*Corresponding author, e-mail address: yichu@mail.stut.edu.tw

actuator). On the other hand, they can transform mechanical deformation into electrical signals; therefore, they can also serve as a sensor. In addition, some piezoelectric materials can be miniaturized to form films or nanowires for further applications. These films are important components of both actuators and sensors in MEMS and microoptical devices, such as micropumps, atomic force microscopy (AFM), ultrasonic micromotors,[1] infrared (IR) detector arrays,[2] micromixers,[3] micromirrors, microrelays,[4] pressure microsensors,[5,6] and stress microsensors.[7] The applications of piezoelectric films are numerous. Recently, piezoelectric materials of high remnant polarization have attracted significant attention because they are very promising for the preparation of memory devices.[8] To realize high-performance MEMS devices, high-quality actuation and sensing materials are demanded.

Currently, most researchers use nonferroelectric materials, such as zinc oxide (ZnO), quartz (SiO_2) and aluminum nitride (AlN), owing to their synthetic process being comparable to the MEMS process. However, lead zirconate titanate (PZT) produces 10-fold larger force and 100-fold higher acoustic power density than these materials.[9]

The following three methods are the most popular for fabricating PZT films: thick-film printing,[10–12] sputtering,[13,14] and sol-gel processing. Thick-film printing can easily yield thick PZT films with thicknesses between 10 and 100 μm. However, this process requires sintering temperatures higher than 850°C to obtain adequate PZT particles. Sputtering is another familiar method of synthesizing PZT films, which are typically less than 1 μm thick. Moreover, postdeposition annealing is required to crystallize the ferroelectric structure of the material, and the chemical compositions of the final product of sputtering are not easily controlled for complex metal oxides, such as PZT. Sol-gel processing is a wet chemical method for the synthesis and processing of inorganic hybrid materials. The author's research is based on this method owing to three advantages. First, this method is convenient for controlling the stoichiometric chemical composition of PZT. Second, sol-gel processing is inexpensive, owing to its 100% usage of precursors without requiring expensive equipment. Finally, it is suitable for mass production and compatible with the device fabrication process in MEMS.

The sol-gel process is one of the most versatile and widely used methods. Nevertheless, the piezoelectric properties of sol-gel-derived PZT films tend to be inferior to those of bulk PZT. This is mainly due to the small grain size of the derived PZT films, which, in turn, results from homogeneous nucleation of many crystalline PZT nuclei during the crystallization process. The piezoelectric effects of the crystalline particles are suppressed upon decreasing grain size. Therefore, homogeneous nucleation should be prevented to achieve optimal piezoelectric properties. The second cause of inferior film properties is the limited film thickness. The thickness of conventional sol-gel processing can hardly reach 1 μm, whereas the charge accumulation owing to the material electric dipole is proportional to the film thickness. In other words, actuation strength and sensing performance are restricted owing to the finite film thickness.

Motivated by the above needs, in this study, two approaches were applied to increase the thickness of the PZT films: rapid thermal treatment[15,16] and precursor concentration modulation.[17,18] Rapid thermal treatment reduced the duration of heating and cooling. This resulted in a lower residue stress within the films and therefore less chances of forming cracks on the film surface. In addition, it reduced the duration of the fabrication

process, enhancing the convenience of batch processing for MEMS applications. The precursor concentration modulation was performed by applying particles to PZT sol. This modulated the concentration of the sol and increased the thickness of the films in each coating. Homogeneous nucleation was thus prevented, and the sizes of the PZT grains increased. In this study, an improved sol-gel method using rapid thermal annealing and a high-concentration PZT sol to achieve a thickness of 10 μm with a crack-free area as large as 16 mm^2 was developed. In addition, the electrical and mechanical performance characteristics of the films were shown.

2. Fabrication of PZT Films

To apply PZT films to MEMS devices, a substrate was prepared by a microfabrication procedure. A 500-nm silicon dioxide film was first thermally wet-grown on a <100> silicon wafer with a thickness of 500 μm. Then a 200-nm silicon nitride film was grown on the top of the silicon dioxide film by low-pressure chemical vapor deposition (LPCVD). An e-beam evaporator was then used to grow the bottom electrode including 50 nm of titanium and 100 nm of platinum. The PZT film was next spun on the bottom electrode and patterned by a conventional photolithography process, BOE (buffered oxide etchant, HF (49%) : FNH_4F (10%) = 6:1) with an AZ4620 mask. A layer of 50 nm of titanium and 100 nm of platinum was deposited and patterned on the PZT film as the top electrode. A lift-off process was applied to the top electrode to expose the bottom electrode for further electrical and mechanical property measurements. The preparation procedure of the whole process is schematically summarized in Fig. 1. Finally, a poling process was carried out by applying 28 V/μm and 100°C to the PZT film for 1 h.

The flow chart of the sol-gel processing for PZT films is shown in Fig. 2. First, PZT sol was prepared using three precursors: $Pb(CH_3COO)_2$, $Zr(C_3H_7O)_4$, and $Ti((CH_3)_2CHO)_4$. The complete synthesis process is published elsewhere.[19] To improve the finite film thickness achieved by conventional sol-gel processing, 0.01 wt% supplementary PZT powder was added to increase the viscosity and concentration of the PZT molecules of the sol. The supplementary particles served as seeds during the PZT annealing process and prevented homogeneous nucleation, enhancing the growth of the PZT grains of the films. The sol was next spin-coated on the substrate at 1500 rpm for 32 s. After the coating, the substrate was initially dried at room temperature for 15 min to evaporate the solvent, and then rapidly heated to 650°C for 15 min to remove organics; in this step, the layer crystallized. The rapid thermal annealing crystallized the films instantly and reduced the chance of cracking caused by thermal mismatch between the PZT films and the substrates. This prevented the films from further shrinking. Moreover, the rapid thermal treatment reduced the time required for the fabrication process. Finally, piezoelectric films of desired thicknesses were achieved by repeating the coating and heating procedures.

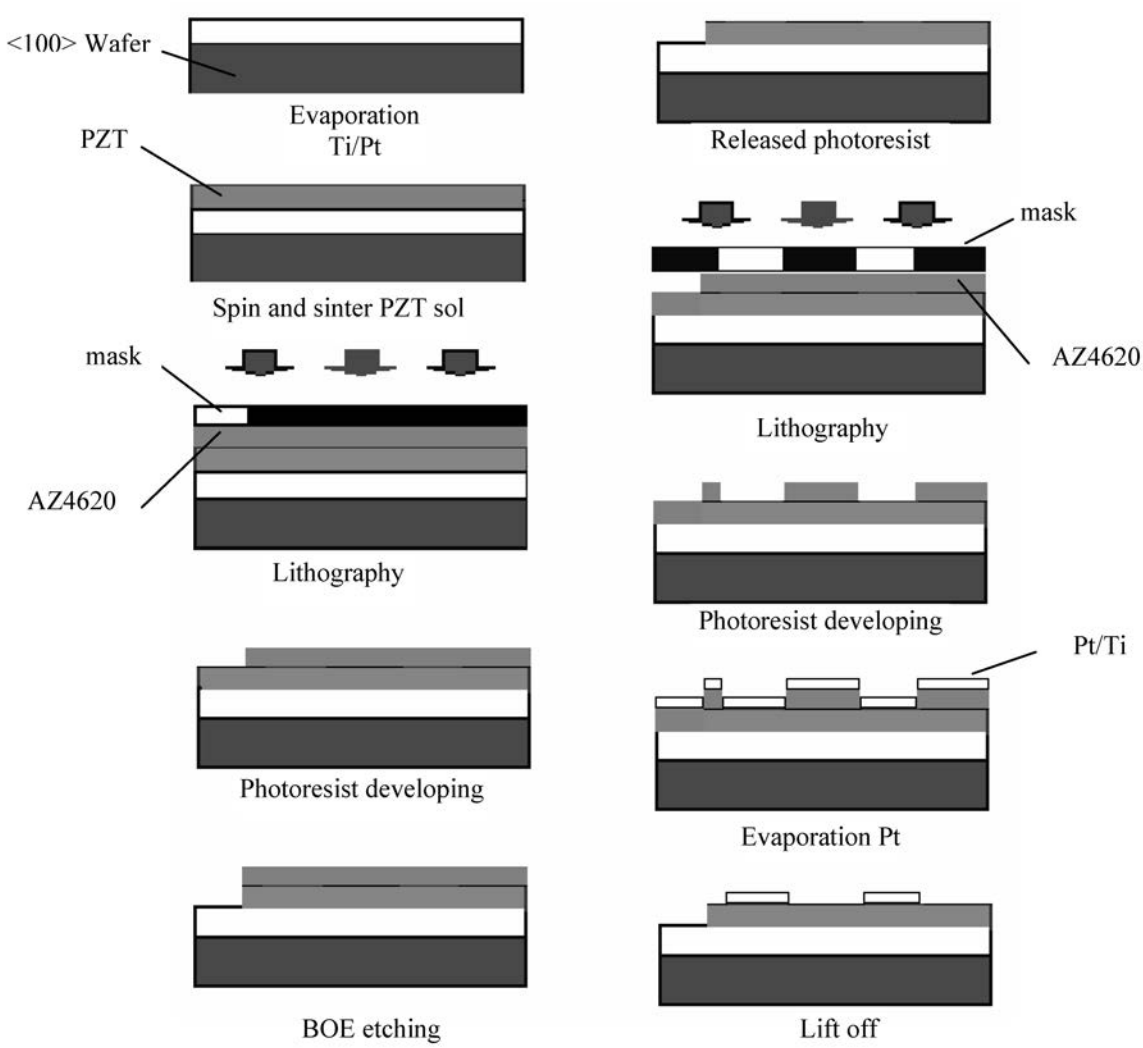

Fig. 1. Preparation procedure of substrate.

3. Characterization of PZT Films

To prove that the sintered film had the correct chemical composition and crystallization pattern, an XRD (X-ray diffraction, Rigaku D/MAX2500, Cu 40 kV 100 mA) examination was performed on one, two, three, and sixteen coating layers of the PZT sol. On the basis of the profile of the XRD spectra shown in Fig. 3, the phase intensity of platinum was found to be high when the number of coating layers was low. On the other hand, the effect of platinum on the phase becomes less significant as the number of coating layers increases.

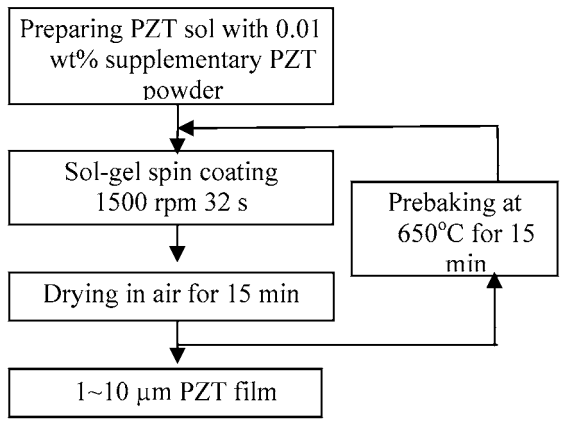

Fig. 2. Preparation procedure of PZT films.

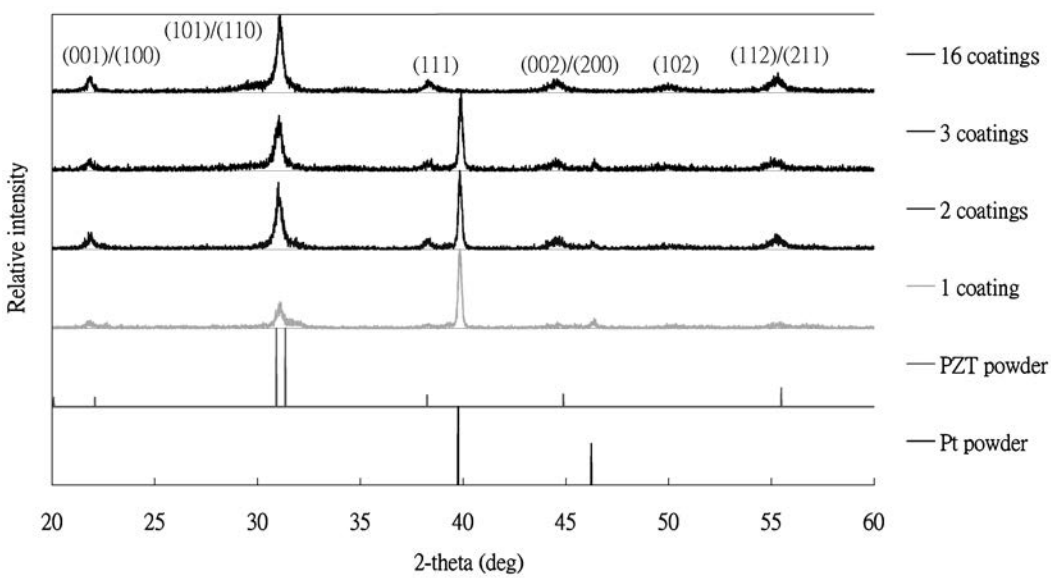

Fig. 3. XRD spectra of PZT and Pt powders, and PZT films with one, two, three and 16 coating layers.

For example, the spectrum intensity of platinum is predominant when the coating number is less than three. This probably results from a thin PZT film that could not prevent the penetration of X-rays to the bottom layer of platinum. However, the platinum phase is absent in the film with 16 coatings. In addition, the X-ray diffraction pattern demonstrates that only the perovskite PZT phase is present in the film and that the pyrochlore phase is absent. The XRD graph shows that the film has a (110) orientation preference texture, which has better piezoelectric properties. Therefore, the sol solution preparation, spin-coating process, and heat treatment for the phase development of PZT films are appropriate.

Figures 4 and 5 show the significance of two techniques applied to improve the conventional sol-gel processing: precursor concentration modulation and rapid thermal annealing. The micrographs in these figures show the film morphologies observed by field emission scanning electron microscope (FE-SEM, PHILIPS, XL-40FEG) and multipurpose scanning electron microscopy (MSEM, JEOL JXA-840). Figure 4 shows micrographs of the PZT films. The film of (a) was synthesized without precursor concentration modulation and that of (b) was synthesized with 0.01 wt% supplementary PZT powder during the sol concentration modification process of this paper, as stated in the fabrication section. In both (a) and (b), the film thickness is 2 μm; however, the grain sizes are 0.8 μm in (a) and 1.5 μm in (b), based on the calculation described in the Heyn procedure (ASTM Standard E 112-88). In addition, the morphology shown in Fig. 4(b) is more solid and compact than that of the image shown in Fig. 4(a). The results reveal that the additional PZT particles serve as seeds for the PZT annealing process; therefore, they prevent homogeneous nucleation and enhance the growth of the PZT grains of the films. The thickness of each coating layer without precursor concentration modulation is only 0.4 μm, whereas that with 0.01 wt% additional PZT particles is 0.6 μm. As a result, supplementary powders increase both grain size and film thickness.

Figure 4(c) shows a surface image of the 10-μm PZT film fabricated by precursor concentration modulation. It shows that the grain size is 14 μm, based on the calculation described in the Heyn procedure. A comparison of the grain sizes in Figs. 4(b) and 4(c) shows that the thicker film could further attain larger grain sizes. The film in Fig. 4(d), which shows a severely cracked surface, was fabricated by conventional heat treatment without rapid thermal annealing. All the films subjected to the conventional heat treatment process show cracked surfaces, irrespective of the number of coating layers. Residual stress is formed during processing primarily due to (1) a thermal mismatch between the bottom electrode Pt and the Si substrate during the PZT annealing process and (2) the volume shrinkage of the PZT film in the x-y direction during devolatilization and crystallization. Typically, residual stress is tensile and on the order of 100 MPa in micromachined membranes and plates. Rapid thermal annealing reduces the time of annealing and therefore suppresses the affects of thermal mismatch and volume shrinkage in the x-y direction. On the basis of the experimental results shown in Figs. 4(c) and 4(d), rapid thermal annealing is considered to prevent film cracking.

Figures 5(a) and 5(b) show cross-sectional SEM images of the films with 3 and 16 coatings, and thicknesses of 2 μm and 10 μm, respectively. On the basis of these SEM images, the structures of the films synthesized by improved sol-gel processing with precursor concentration modulation and rapid thermal annealing are determined to be

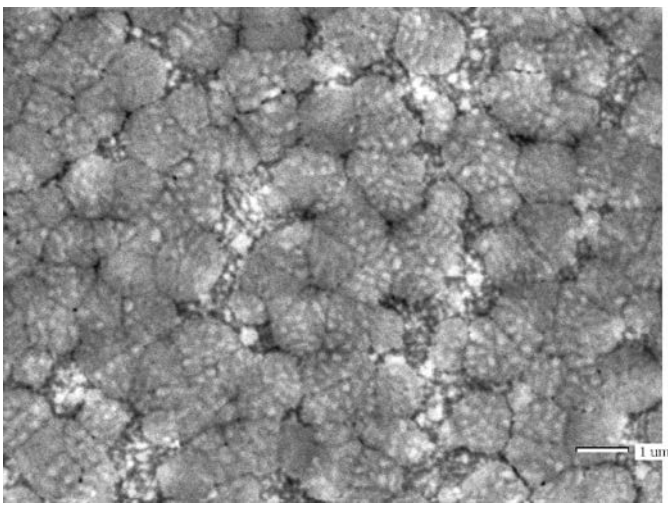

(a)

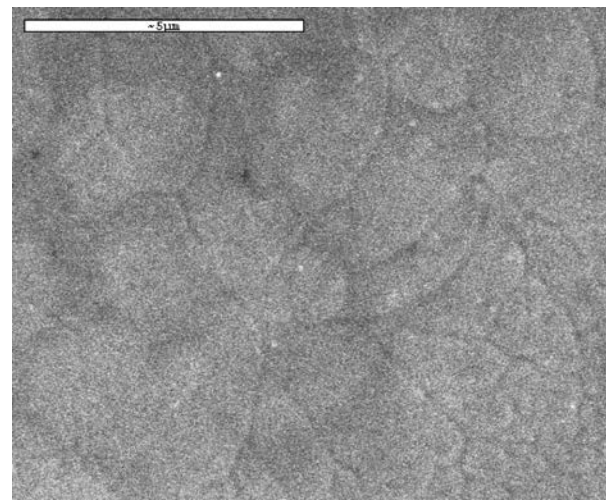

(b)

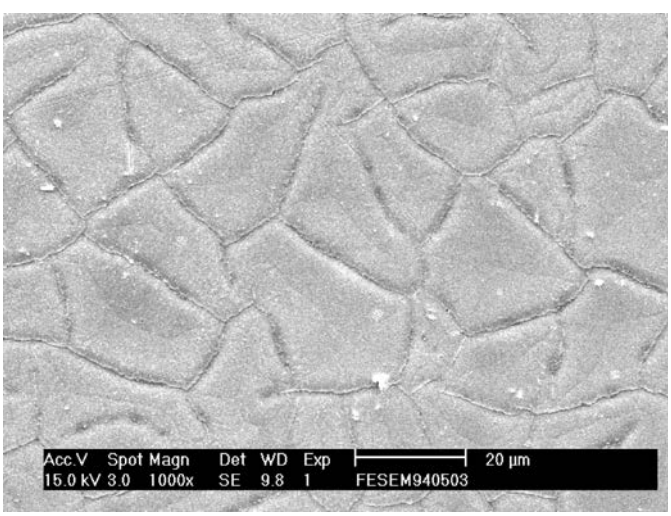

(c)

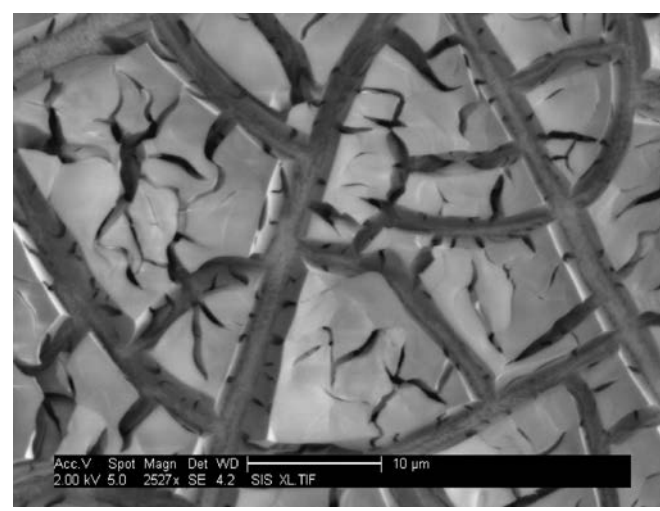

(d)

Fig. 4. Surface morphologies of PZT films fabricated (a) without precursor concentration modulation, film thickness=2 μm (scale bar of 1 μm), (b) with precursor concentration modulation, film thickness=2 μm (scale bar of 5 μm), (c) with precursor concentration modulation, film thickness=10 μm (scale bar of 20 μm), and (d) with conventional heat treatment without rapid thermal annealing (scale bar of 10 μm).

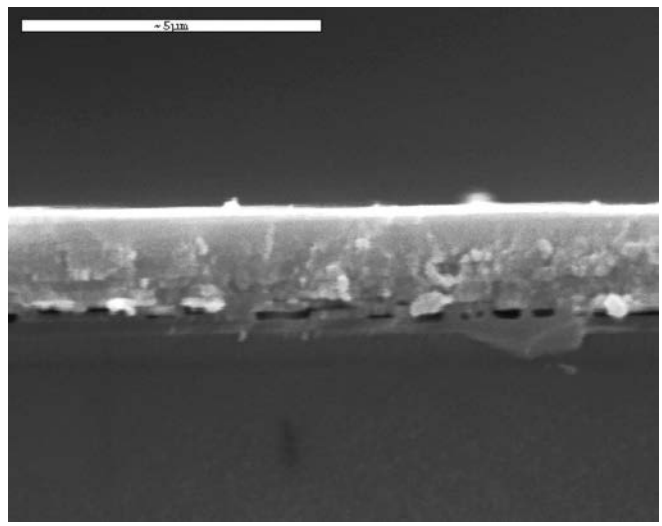

(a)

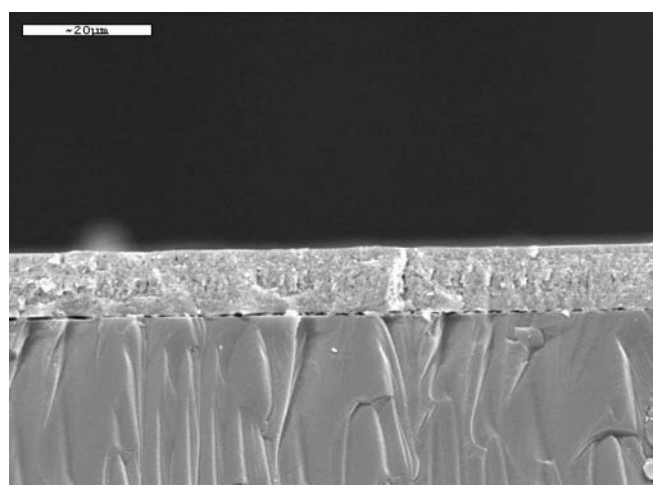

(b)

Fig. 5. Cross-sectional SEM images of (a) 2-μm PZT film (scale bar of 5 μm) and (b) 10 μm PZT thin film (scale bar of 20 μm).

dense and crack-free. The thickness of each coating is approximately 0.6 μm, which is much larger than those of the PZT films fabricated by conventional sol-gel processing, e.g., a one-half-micron-thick PZT film resulting from a 3-layer coating process.[20]

Figure 6 shows the PZT surface roughness measured by atomic force microscope (AFM, Veeco, CP). Within a surface area of 5×5 μm, the average roughness is 2.2 nm, and the root mean square (rms) roughness is 2.9 nm. The surface is satisfactorily smooth and appropriate for processing for further MEMS device applications.

The electric properties of the films were also evaluated using a dielectric constant and hysteresis loops. In general, the dielectric constant at 1 kHz ranges from 143 to 149, and from 157 to 162, for the films of 2.2 μm and 7.2 μm thicknesses that are listed in Table 1, respectively. Thicker films could attain a higher dielectric constant, and a higher frequency yields a lower dielectric constant.

The hysteresis loops of the 2.2- and 7.2-μm-thick PZT films are shown in Fig. 7. These loops were both measured at a fixed AC electric field of 20 V/mm, with a reference capacitor of 1 μF. The coercive field (*E*c) and remnant polarization (*P*r) values obtained from the P-E hysteresis loop are 3.01 V/μm and 1.63 μC/cm^2, and 6.44 V/μm and 3.63 μC/cm^2, for film thicknesses of 2.2 and 7.2 μm, respectively. Figure 7 shows that a thicker film demonstrates higher Pr and Ec values. These experimental measurements are in accordance with the theory that a thicker film has better ferroelectric properties.

4. PZT Films as Actuators and Sensors

In addition to correct piezoelectric crystallization, morphology observation and electrical property measurements, the dynamic performance of the piezoelectric films was investigated. The investigation of the dynamic performance consists of two parts: actuation and sensing tests.

The first step is to demonstrate that the PZT film has a sufficient actuation strength to be used in silicon-based structures. The setup for the actuation tests is shown in Fig. 8. The specimen was cut to dimensions of 40×7 mm using a beam. The top electrode was patterned with dimensions of 4×4 mm. One end of the beam was clamped and the other end was maintained free as a cantilever beam. The setup for the actuation tests consisted of a function generator (Motech, FG 503), a power amplifier (Piezotronics, PCB790), a digital oscilloscope (Tektronix, TDS2014) and a fiber-optic measurement system (MTI Instruments, MTI 2000). First, the function generator drove the PZT film with the aid of the power amplifier. Also, the photonic sensor monitored the vibration of the cantilever. In the meantime, all the signals were recorded by a digital oscilloscope, as shown in Fig. 9.

Figure 9 shows that the vibration signal of the beam was driven by a 6.5-μm-thick PZT film with an actuation area of 4×4 mm. The first trace is the voltage from the function generator. The second trace is one-twentieth of the voltage in the PZT film. The last trace is the response measured by the photonic sensor. The system was driven at the first bending mode of the specimen at 346 Hz. The vibration amplitude at the tip of the specimen was 2.4 μm with a driving voltage of 196 V_{pp}. In addition, the frequencies of the vibration and driving signal were identical to those of the source from the function generator in the first trace. The results in Fig. 9 show that a 4×4×6.5 μm PZT film is adequately strong to serve as an actuator to drive a 40×7×0.5 mm silicon beam with a vibration amplitude as large as 2.4 μm.

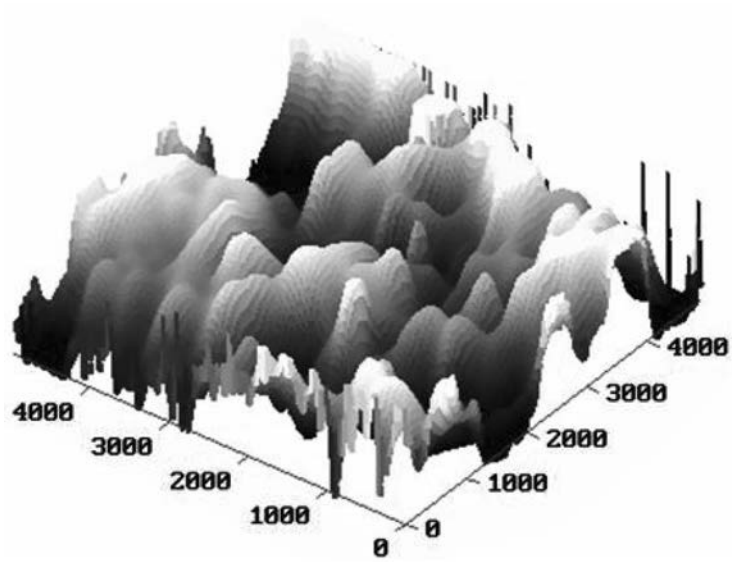

Fig. 6. AFM surface micrograph of PZT film surface.

Table 1
Experimental measurements of capacitance and dielectric constant for PZT films with area of 4×4 mm.

		Frequency (KHz)	Capacitance (nF)	Dielectric constant
2.2 μm	Pad 1	1	9.63	149
		10	9.16	141
	Pad 2	1	9.23	143
		10	8.88	137
	Pad 3	1	9.58	148
		10	9.18	142
7.2 μm	Pad 1	1	3.06	157
		10	2.95	148
	Pad 2	1	3.01	157
		10	2.90	151
	Pad 3	1	3.18	162
		10	3.05	156

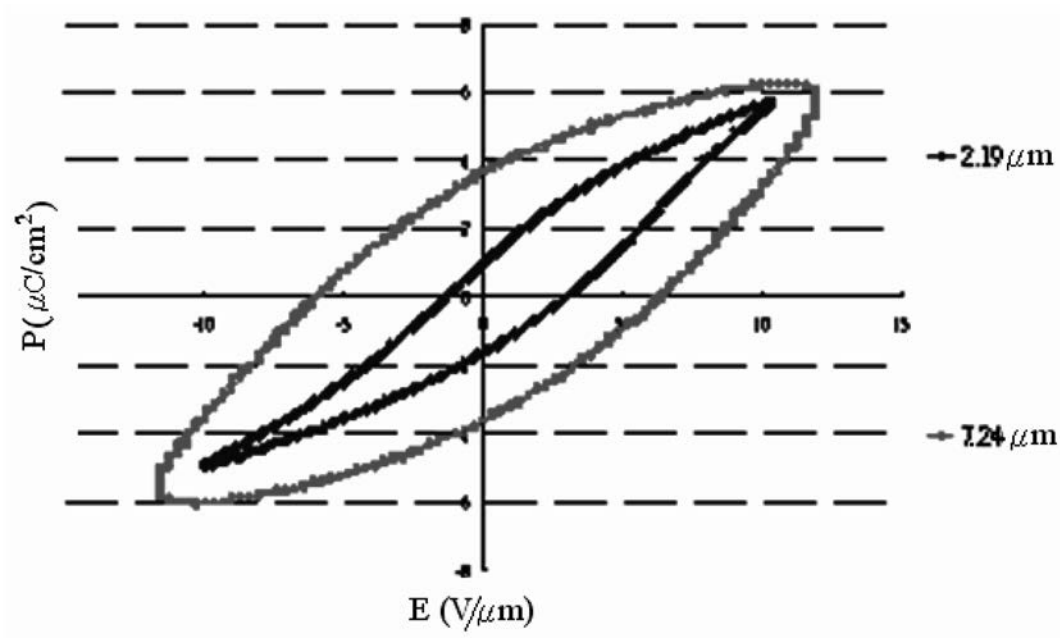

Fig. 7. Hysteresis loops of 2.2- and 7.2-μm-thick PZT films.

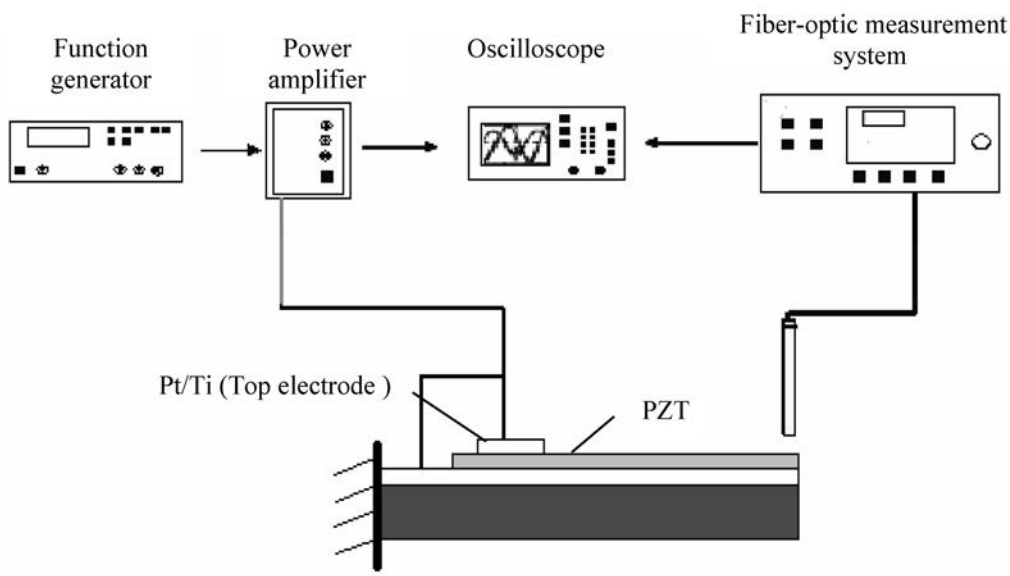

Fig. 8. Schematic diagram of experimental setup for actuation tests on PZT film.

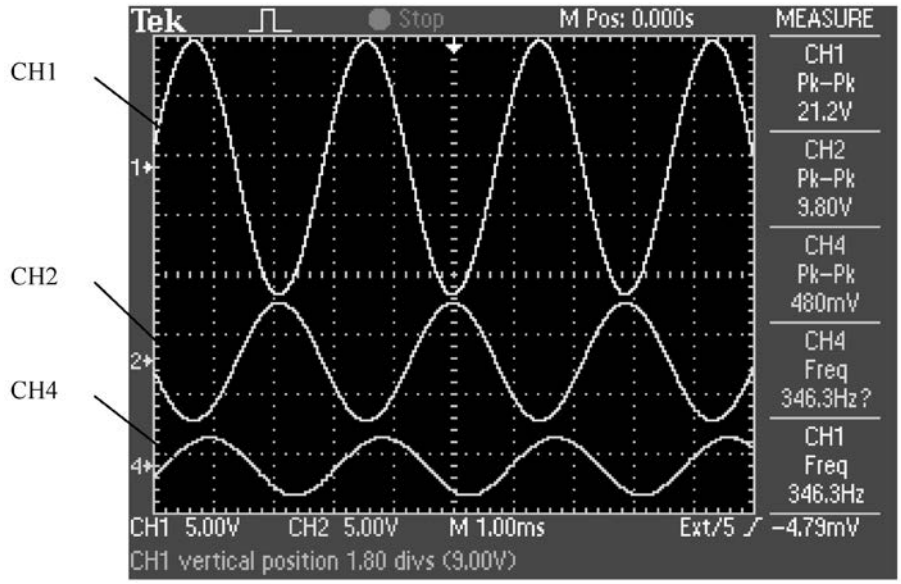

Fig. 9. Actuation tests on 6.5-μm PZT film at first bending mode recorded by oscilloscope (CH1: excitation from function generator, CH2: driving voltage divided by 20, CH4: vibration signal detected by photonic sensor).

The same specimen, namely, the 6.5-μm-thick PZT film used in the actuation tests was also chosen for sensing tests. Sensing tests were carried out using a function generator, the power amplifier, a shaker (PCB Piezotronics, Inc., AVC-712A01) and a photonic sensor, as shown in Fig. 10. With the aid of the function generator and power amplifier, the shaker served as a vibration source to excite the specimen. The photonic sensor measured the vibration of the specimen at the corner of the free end. Without using a charge amplifier, the electric signal generated by the PZT film owing to specimen vibration was recorded by the digital oscilloscope.

Figure 11 shows one of the test results recorded by an oscilloscope. The first trace is the driving voltage from the function generator, which is 10.4 V_{pp} at 347 Hz (the first bending mode of the specimen). The second trace is the driving voltage from the amplifier, divided by a factor of 20, in the shaker. The third trace is the voltage measured from the PZT film responding to the vibration of the specimen. The amplitude is 3.12 V_{pp}. The response is sinusoidal and its frequency is identical to the driving frequency. This indicates that the system is in the linear range. This also demonstrates that the PZT thin film can serve as an effective sensor for small structures. Finally, the last trace is the response measured from the photonic sensor for reference. On the basis of the experimental results, the frequency of the PZT sensing signal was determined to be the same as the driving frequency and the amplitude was proportional to the excitation voltage.

The dynamic performance of the 4 mm×4 mm×6.5 μm PZT film (on the 40×7× 0.5 mm silicon beam) both as an actuator and a sensor is summarized in Table 2. In the actuation

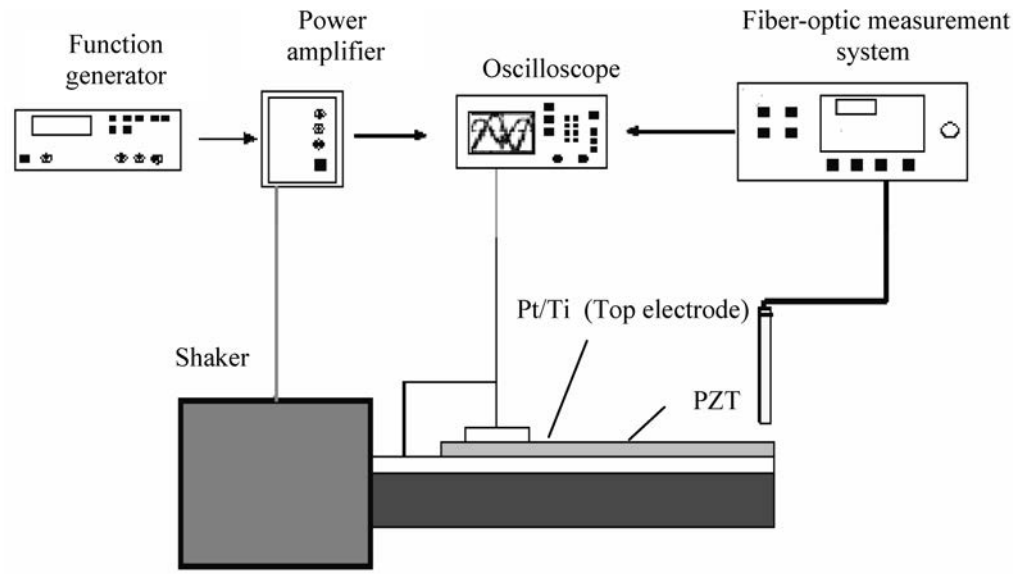

Fig. 10. Schematic diagram of experimental setup for PZT sensing tests.

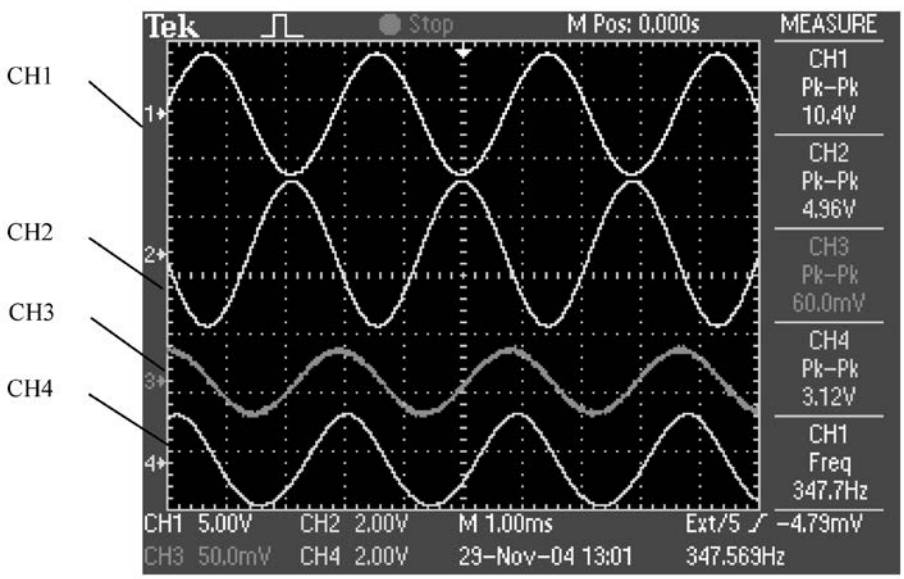

Fig. 11. Sensing tests on 6.5-μm PZT film at 347 Hz recorded by oscilloscope (CH1: excitation from function generator, CH2: amplified driving signal, CH3: signal of PZT film, CH4: reference signal from photonic sensor).

Table 2
Dynamic performance of cantilever specimen in experiments and theory.

	Actuator (excitation voltage into PZT film, *V*pp=196 V)				Sensor (excitation voltage into shaker, *V*pp=96 V)			Theory
Mode	Tip center		Corner		Freq.	Amp.	Signal*	Freq.
	Freq.	Amp.	Freq.	Amp.				
First bending	346.4	2.40	345.8	2.20	347.6	15.6	60	364.4
Second bending	2300	0.96	2303	0.66	–	–	–	2283.3

Units: Freq. (Hz), Amp. (μm)
* The sensing response of the PZT film is in units of mV.

tests, the resonance frequencies were measured at the tip center and corner of the beam to ensure that the first and second modes were indeed the bending modes. The frequencies of the first two modes were compared with the theoretical results obtained by using the Euler-Bernoulli beam theory.[21] This comparison demonstrates that the experimental results are similar to the theoretical data with an error of 5.19% at the first resonance.

5. Conclusions

PZT films with thicknesses between 1 and 10 μm for MEMS applications have been successfully fabricated by the improved sol-gel method using two techniques: precursor concentration modulation and rapid thermal annealing. A 0.01 wt% additional PZT powder could increase both the size of grains and the thickness of single coating layers. The grain sizes and thicknesses of a single coating layer are 1 and 5 μm, and 0.4 and 0.6 μm/coating, for the conventional sol-gel method and improved sol-gel method with precursor concentration modulation, respectively. In addition, the films synthesized by precursor concentration modulation are more solid and compact than those without the modulation. Rapid thermal annealing is required to attain crack-free films. The films obtained by conventional heat treatment result in a severely cracked surface.

Electrical properties were assessed by the observation of the dielectric constant and hysteresis curves. The experimental results demonstrated that the dielectric constant was approximately 160 at 1 kHz. The remnant polarization and coercive field of the PZT ferroelectric capacitors were about 3.63 $\mu C/cm^2$ and 64.4 kV/cm, respectively.

A method of characterizing the dynamic performance of PZT films was also developed. For further applications of the films in MEMS communities, the films were first grown on $Pt/Ti/Si_3N_4/SiO_2/Si$ substrates. Secondly, the PZT films were patterned by a standard photolithography process with BOE wet etching and AZ4620 photoresist protection. Finally, both the actuation and sensing performance characteristics of the films on the

MEMS-based specimen were experimentally tested, and theoretical results obtained by considering the Euler-Bernoulli beam theory verified the dynamic performance. On the basis of the results, the feasibility of using PZT films fabricated by the improved sol-gel method as sensors and actuators for micro- and meso-structures was successfully demonstrated.

Acknowledgements

The author gratefully acknowledges the support for this research given by the National Science Council (grant NSC 93-2212-E-218-001). The author also thanks National Nano Device Laboratories and Center for Micro/Nano Technology Research for fabrication support.

References

1 P. Muralt, M. Kohli, T. Maeder, A. Kholkin, K. G. Brooks, N. Setter and R. Luthier: Sens. Actuators, A **48** (1995) 157.
2 B. Willing, M. Kohli, P. Muralt, N. Setter and O. Oehler: Sens. Actuators, A **66** (1998) 109.
3 Z. Yang, H. Goto, M. Matsumoto and R. Maeda: Electrophoresis **21** (2000) 116.
4 H. Kueppers, T. Leuerer, U. Schnakenberg, W. Mokwa, M. Hoffmann, T. Schneller, U. Boettger and R. Waser: Sens. Actuators, A **97** (2002) 680.
5 E. Defay, C. Millon, C. Malhaire and D. Barbier: Sens. Actuators, A **99** (2002) 64.
6 T. Kanda, T. Morita, M. Kurosawa and T. Higuchi: Proc. IEEE Micro Electro Mech. Sys. (MEMS, Heidelberg, 1998) p. 378.
7 S. Hunt, A. Rudge, M. Carey, M. Parfitt, J. Geoffrey and I. Huntsman: Smart Materials and Structures **11** (2002) 617.
8 N. Inoue, T. Takeuchi and Y. Hayashi: IEEE Trans. on Electron Dev. **49** (2002) 1572.
9 S. T.-McKinstry and P. Muralt: Integ. Ferroelectr. **17** (1997) 297.
10 K. Yao, X. He, Y. Xu and M. Chen: Sens. Actuators, A **118** (2005) 342.
11 K. Yao, X. He, Y. Xu and M. Chen: Int. Soc. Opt. Eng. **5389**, Smart Materials and Structures 2004 (SPIE, San Diego, 2004) p. 108.
12 V. Walter, P. Delobelle, P. Le Moal, E. Joseph and M. Collet: Sens. Actuators, A **96** (2002) 157.
13 S. B. Krupanidhi, N. Maffei, M. Sayer and K. El-Assal: Ferroelectrics **51** (1983) 93.
14 W. L. Chang: Ceramics Int. **31** (2005) 461.
15 J. Li, L. Zhang, X. Yao and J. Wang: Ceram. Int. **30** (2004) 1509.
16 C. D. E. Lakeman, Z. Xu, D. A. Payne: IEEE Int. Symp. Appl. Ferroelectrics (IEEE, Pennsylvania, 1994) p. 404.
17 Y. T. Kwon, I. M. Lee, W. I. Lee, C. J. Kim and I. K. Yoo: Mater. Res. Bull. **34** (1999) 749.
18 Z. Chen, C. Yang, S. Wang and B. Yang: J. Mater. Sci. **17** (2006) 51.
19 Y. C. Hsu, C. C. Wu, C. C. Lee, G. Z. Cao and I. Y Shen: Sens. Actuators, A **116** (2004) 369.
20 S. W. Bae, H. H. Park and T. S. Kim: Sens. Actuators, A **125** (2006) 548.
21 I. Daniel: Engineering Vibration (Prentice-Hall, Inc., New Jersey, 2001) Chaps. 6 and 8.